

# Accelerated Newton-Raphson GRAPE methods for optimal control

David L. Goodwin<sup>1,2,\*</sup> and Mads Sloth Vinding<sup>3,†</sup>

<sup>1</sup>Chemistry Research Laboratory, University of Oxford, Mansfield Road, Oxford OX1 3TA, UK

<sup>2</sup>Institute for Biological Interfaces 4 – magnetic resonance,  
Karlsruhe Institute for Technology (KIT), Karlsruhe, Germany

<sup>3</sup>Center of Functionally Integrative Neuroscience (CFIN),  
Department of Clinical Medicine, Faculty of Health, Aarhus University, Denmark

(Dated: August 19, 2022)

A Hessian based optimal control method is presented in Liouville space to mitigate previously undesirable polynomial scaling of computation time. This new method, an improvement to the state-of-the-art Newton-Raphson GRAPE method, is derived with respect to two exact time-propagator derivative techniques: auxiliary matrix and ESCALADE methods. We observed that compared to the best current implementation of Newton-Raphson GRAPE method, for an ensemble of 2-level systems, with realistic conditions, the new auxiliary matrix and ESCALADE Hessians can be 4-200 and 70-600 times faster, respectively.

PACS numbers: 02.30.Yy, 02.60.Pn, 03.67.-a, 87.80.Lg

Keywords: Optimal Control, Hessian, Newton-Raphson, GRAPE

## I. INTRODUCTION

The problem of transferring the state of a dynamical system to a desired target state while minimising the remaining distance and costs is often solved with optimal control theory [1, 2]. Applications include quantum sensing [3–6], quantum computing [7–9], and nuclear magnetic resonance (NMR) spectroscopy [10–13] and imaging (MRI) [14, 15].

A number of different approaches to optimal control (OC) has lead to the development of different methods: Lagrangian methods [16–19]; minimal-time OC [10]; gradient ascent pulse engineering (GRAPE) [12]; sophisticated gradient-free searches [20, 21]; Krylov-Newton methods [22]; OC with a basis of analytic controls [23, 24]; a tensor product approach for large quantum systems [25]. The method outlined in this work is based on a piecewise-constant control pulse approximation [26–29] of GRAPE [12, 30, 31] using a gradient following numerical optimisation.

Although finding an optimal solution to the problem of controlling a single 2-level system from a defined initial system state to a desired target state, a *state-to-state* problem, is considered straight-forward and computationally inexpensive with modern methods and computing power; an OC problem can become numerically and computationally arduous [32], particularly for applications that account for practical hardware configurations and limitations [11, 33, 34]. Additionally, the computational expense can increase dramatically when optimising over an ensemble of systems, such as the case in solid-state nuclear magnetic resonance [13, 35, 36], where the ensemble also includes crystalline orientations of a powder average [37]. The particular application of OC of interest to the authors is that of a neural network based method for MRI [38–40] and a method of morphic OC [41, 42], requiring hundreds of thousands of optimised pulse shapes to form their optimal libraries.

Keeping the example of MRI, the utility of OC is highlighted when considering the legal constraints of power deposition safeguards [43] and the obvious financial rewards of reducing the time a patient stays inside the MRI machine.

Modern techniques can mitigate protracted numerical convergence with a quadratically convergent optimisation method, requiring the calculation of a Hessian matrix, giving a large saving in the number of required serial optimisation iterations [31, 35, 44]. However, it is known within the community that calculation of the Hessian matrix does not scale well to a control problem with a large number of controllable amplitudes [45] (also shown in Fig. 1).

This communication presents a jump in computational efficiency of multiple-orders of magnitude with a rework of the original method, devised to calculate the exact Hessian matrix [31, 35, 46], and the recently published exact, matrix-free, method of efficient spin control using analytical Lie algebraic derivatives (ESCALADE) [44]. The manuscript will present the mathematical formulation of these exact Newton-Raphson GRAPE methods in the irreducible spherical-tensor basis of a Liouville space and show a newly devised method to calculate the Hessian matrix with  $\mathcal{O}(N)$  scaling, compared to the previous  $\mathcal{O}(N^2)$  scaling (Fig. 1). Results show the comparative speedup of this method to the original in the context of state-to-state MRI problems, requiring a generalisation of the ESCALADE method with calculations of optimal z-controls.

## II. EXACT NEWTON-RAPHSON OPTIMAL CONTROL

### A. Optimal control in Liouville space

A quantum system can be described by a density operator,  $\hat{\rho}(t)$ ; a time-dependent system state. The evolution of this state is dictated by the Liouville-von Neumann equation,

$$\frac{\partial}{\partial t} \hat{\rho}(t) = -i[\hat{H}(t), \hat{\rho}(t)] \quad (1)$$

\* david.goodwin@partner.kit.edu

† msv@cfi.au.dk

where  $\hat{H}(t)$  is a time-dependent Hamiltonian, an operator in a Hilbert space with a spectrum of allowed energy levels. The usual factor of  $\hbar$  is dropped here, resulting in the eigenspectrum of  $\hat{H}$  expressed in angular frequency units. The methods presented in this manuscript are particular to a Liouville space, also named the adjoint representation[30, 31, 35]. A system state in a Liouville space is represented by a vector,  $|\hat{\rho}\rangle$ , obtained by stacking columns of the density operator  $\hat{\rho}$  with Eq. (1) becoming

$$\frac{\partial}{\partial t}|\hat{\rho}(t)\rangle = -i\hat{L}(t)|\hat{\rho}(t)\rangle, \quad \hat{L}(t) \triangleq \mathbb{1} \otimes \hat{H}(t) - \hat{H}(t)^\top \otimes \mathbb{1} \quad (2)$$

where the identity matrix,  $\mathbb{1}$ , and Hamiltonian have the same dimension.

The form of a bilinear control problem is to split that which is controllable, *the control*, from that which is not, *the drift*. The Liouvillian for a control problem with x-, y-, and z-controls on a 2-level system can be written as

$$\hat{L}(t) = \underbrace{\omega \hat{L}_z}_{\text{drift}} + \underbrace{c_x(t)\hat{L}_x + c_y(t)\hat{L}_y + c_z(t)\hat{L}_z}_{\text{control}} \quad (3)$$

where the angular frequency  $\omega$  is the time-independent resonant frequency offset,  $c_{x,y,z}(t)$  are time-dependent control amplitudes, and  $\hat{L}_{x,y,z}$  are Pauli matrices of a Liouville space.

The OC method of GRAPE [12] uses piecewise constant control pulses, where control pulses are constant over a small time interval,  $\Delta t$  [28, 29]:

$$c_k(t) \rightarrow [c_{k,1} \ c_{k,2} \ \cdots \ c_{k,N}], \quad k \in \{x, y, z\} \quad (4)$$

using the notation  $c_{k,n} \equiv c_k(t_n)$  for convenience, and  $t_N = N\Delta t$ . This discrete formulation allows numerical solution to Eq. (2), given an initial state of the system  $|\hat{\rho}_0\rangle$ , through time-ordered propagation

$$|\hat{\rho}_N\rangle = \hat{P}_N \hat{P}_{N-1} \cdots \hat{P}_2 \hat{P}_1 |\hat{\rho}_0\rangle \quad (5)$$

where  $\hat{P}_n$  are time-propagators of an isolated time-slice and are defined through the exponential map

$$|\hat{\rho}_n\rangle = \hat{P}_n |\hat{\rho}_{n-1}\rangle, \quad \hat{P}_n = e^{-i\hat{L}_n \Delta t} \quad (6)$$

The matrix exponential of Eq. (6) usually calculated with the Padé approximant, Taylor series, or Krylov propagation [35].

An additional method to calculate the time-propagators of a 2-level system is by explicitly calculating the elements of the matrix. In a spherical-tensor basis, this matrix is the Wigner-matrix [47]:

$$\hat{P}_n = \begin{bmatrix} \alpha^2 & \sqrt{2}\alpha\beta & \beta^2 \\ -\sqrt{2}\alpha\beta^* & \alpha\alpha^* - \beta\beta^* & \sqrt{2}\alpha^*\beta \\ \beta^{*2} & -\sqrt{2}\alpha^*\beta^* & \alpha^{*2} \end{bmatrix} \quad (7)$$

which is formulated in terms of the complex elements

$$\alpha = \cos \phi + i \frac{z}{r} \sin \phi, \quad \beta = \frac{y}{r} \sin \phi + i \frac{x}{r} \sin \phi, \quad (8)$$

where the shorthands  $x = c_{x,n}$ ,  $y = c_{y,n}$ , and  $z = c_{z,n} + \omega$  are used,  $\phi = \frac{1}{2}r\Delta t$  is a polar angle of rotation, and  $r = \sqrt{x^2 + y^2 + z^2}$  is the polar radius.

As a notational convenience for what follows, the following *effective propagators* are defined as the effect of the pulse between time slices  $m$  and  $n$ :

$$\mathbf{U}_m^n \triangleq \hat{P}_n \hat{P}_{n-1} \cdots \hat{P}_{m+1} \hat{P}_m, \quad \forall (1 \leq m \leq n \leq N) \quad (9)$$

where a backward (time-reversed) propagation can be denoted by  $\mathbf{U}_n^m = \mathbf{U}_m^{n\dagger}$ .

Optimal control requires a metric to optimise; the *fidelity* [12, 48],  $\mathcal{F}$ , a measure how well the pulses perform a desired control task. The task of the OC problem is to find a set of control amplitudes,  $c_{x,y,z}(t)$ , that maximise the fidelity e.g. the real part of an inner product:

$$\max_{c_{x,y,z}(t)} (\mathcal{F}) = \max_{c_{x,y,z}(t)} \left( \text{Re} \langle \hat{\sigma} | \mathbf{U}_1^N | \hat{\rho}_0 \rangle \right) \quad (10)$$

This form of the fidelity metric is defined in terms of state-to-state problems, where a system is in a defined initial state,  $|\hat{\rho}_0\rangle$ , and the control task is to take this state to a desired one,  $|\hat{\sigma}\rangle$ . With the notation introduced in Eq. (9),  $\mathbf{U}_1^N$  is interpreted as the effective propagator over the shaped pulse. In addition to Eq. (5), the system is propagated backwards from the desired target state,

$$|\hat{\chi}_n\rangle = \hat{P}_n^\dagger \hat{P}_{n+1}^\dagger \cdots \hat{P}_{N-1}^\dagger \hat{P}_N^\dagger |\hat{\sigma}\rangle \quad (11)$$

which is termed the *adjoint state* of the control problem [35].

GRAPE is a gradient following numerical optimisation method and requires derivatives of the fidelity with respect to the controls. In turn, this requires the directional propagator derivatives,  $D_{k,n}^a$ ; with the subscripts  $k$  denoting the derivative in the direction of  $\hat{L}_k$  and  $n$  denoting the derivative operating on the time-propagator  $\hat{P}_n$ . For each time-slice,  $n$ , and for each control direction  $\hat{L}_k \in \{\hat{L}_x, \hat{L}_y, \hat{L}_z\}$ , the  $a^{\text{th}}$  order derivative takes the form

$$\nabla^a \mathcal{F}(c_{k,n}) = \text{Re} \left\langle \hat{\chi}_{n+1} \left| \underbrace{D_{k,n}^a}_{N \text{ times}} \hat{\rho}_{n-1} \right. \right\rangle, \quad (12)$$

where bra-ket notation explicitly shows vector structures i.e.  $|D_{k,n}^a \hat{\rho}_{n-1}\rangle = D_{k,n}^a |\hat{\rho}_{n-1}\rangle$ . The number of forward and backward propagations is indicated for each control channel to produce a gradient vector,  $\nabla \mathcal{F}$ , or the diagonal elements of a Hessian matrix,  $\nabla^2 \mathcal{F}$ .

This is sufficient for a fidelity gradient, scaling linearly with  $N$ , but a fidelity Hessian also requires mixed second order derivatives [31], where the off-diagonal Hessian elements are

$$\nabla^2 \mathcal{F}(c_{k,n}, c_{j,m}) = \text{Re} \left\langle \hat{\chi}_{n+1} \left| \underbrace{D_{k,n}^a}_{N \text{ times}} \underbrace{\mathbf{U}_{m+1}^{n-1} |D_{j,m}^b \hat{\rho}_{m-1}\rangle}_{\frac{1}{2} N(N-1) \text{ times}} \right. \right\rangle \quad (13)$$

Clearly, the form of Eq. (13) has a central propagator that cannot be absorbed into the bra or ket because it depends on both

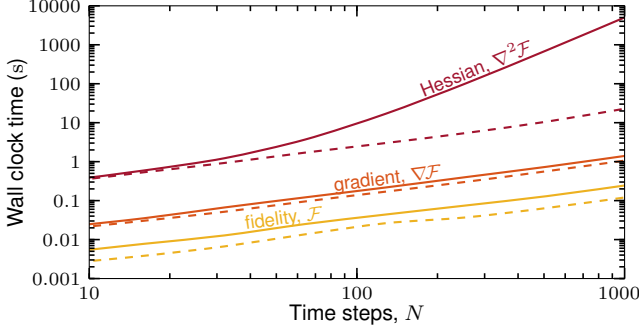


FIG. 1. Average wall-clock time of fidelity, gradient, and Hessian for increasing  $N$ . Solid lines show the Newton-Raphson GRAPE method [31] and dashed lines show the proposed *accelerated* Newton-Raphson GRAPE method. Both methods use the auxiliary matrix method [46] to calculate propagator derivatives.

$t_n$  and  $t_m$ , and therefore the computation scales polynomially with  $\frac{1}{2}N(N-1)$  (the factor  $\frac{1}{2}$  comes from the symmetric property of a Hessian [35]). This is known within the OC community [45] and is highlighted in Fig. 1. The linear plots of the fidelity and gradient, on log-log axes, show these calculations are efficient with increasing  $N$ , whereas the Hessian calculation time is not linear on these log-log axes. The subject of this manuscript is to mitigate this undesirable scaling, resulting in a linearly scaling Hessian calculation (dashed lines in Fig. 1), after the following section outlines calculation of directional propagator derivatives.

## B. Directional propagator derivatives with auxiliary matrices

As has been published previously [31, 35, 46], exact propagator derivatives required by Eq. (12) and (13) can be calculated by exponentiating an auxiliary matrix: resulting in an upper triangular block matrix [49] with a time-propagator,  $\hat{P}_n$ , on the block diagonal, and with the directional derivative of that propagator, calculated in the direction of a control operator, in the upper triangular block. The first and second order propagator derivatives can be extracted from

$$\exp \begin{bmatrix} \mathbf{A}_n & \mathbf{C}_j & \mathbf{0} \\ \mathbf{0} & \mathbf{A}_n & \mathbf{C}_k \\ \mathbf{0} & \mathbf{0} & \mathbf{A}_n \end{bmatrix} = \begin{bmatrix} \hat{P}_n & D_{j,n} & \frac{1}{2}D_{jk,n}^2 \\ \mathbf{0} & \hat{P}_n & D_{k,n} \\ \mathbf{0} & \mathbf{0} & \hat{P}_n \end{bmatrix} \quad (14)$$

where the block matrix is formed from  $\mathbf{A}_n = -i\hat{L}_n\Delta t$ , as in Eq. (6), and  $\mathbf{C}_k = -i\hat{L}_k\Delta t$  are functions of the control operators with  $j, k \in \{x, y, z\}$ .

## C. Directional propagator derivatives with ESCALADE

Whereas Eq. (14) is exact, the matrix exponential is expensive. Foroozandeh and Singh recently devised a method that is free from this expensive matrix exponential calculation, in the

OC method of Efficient Spin Control using Analytical Lie Algebraic Derivatives (ESCALADE) [44]. This method can also be extended with interaction propagator splitting [50].

The efficient method of ESCALADE to calculate the directional derivatives in Eqs. (12) and (13), in this single spin model, is to construct a matrix with rows containing all elements needed to construct the propagator derivatives

$$\begin{bmatrix} \Theta_x \\ \Theta_y \\ \Theta_z \end{bmatrix} = \text{vec}[\mathbf{1}] + \frac{\sin^2 \phi}{\phi r} \text{vec}[\mathbf{S}] + \frac{2\phi - \sin 2\phi}{2\phi r^2} \text{vec}[\mathbf{S}^2] \quad (15)$$

where  $\text{vec}[\mathbf{1}]$  is a vectorised identity matrix, with a vectorisation operation on a matrix  $\mathbf{A}$  such that  $\mathbf{A} = \text{vec}^{-1}[\text{vec}[\mathbf{A}]]$ . The skew-symmetric matrix  $\mathbf{S}$  is

$$\mathbf{S} = \begin{bmatrix} 0 & z & -y \\ -z & 0 & x \\ y & -x & 0 \end{bmatrix} \quad (16)$$

and the symmetric matrix  $\mathbf{S}^2$  is calculated algebraically. In turn, the directional propagator derivatives can be written as

$$D_{k,n} = \hat{P}_n \left[ \text{vec}^{-1}[\Sigma \Theta_k] \right] \quad (17)$$

$$D_{jk,n}^2 = \hat{P}_n \left[ \text{vec}^{-1}[\Sigma \Theta_{jk}] \right] + \hat{P}_n \left[ \text{vec}^{-1}[\Sigma \Theta_j] \right] \left[ \text{vec}^{-1}[\Sigma \Theta_k] \right] \quad (18)$$

where  $\Sigma = [\text{vec}[\mathbf{C}_x] \text{vec}[\mathbf{C}_y] \text{vec}[\mathbf{C}_z]]$  is a 3-column matrix to be multiplied with the 3-row matrix of  $\Theta_k$ . Using a similar notation to Eq. (15), the  $\Theta_{jk}$  matrices required by the second order derivatives in Eq. (18) are

$$\begin{bmatrix} \Theta_{jx} \\ \Theta_{jy} \\ \Theta_{jz} \end{bmatrix} = \frac{\cos(2\phi) - 1}{r^2} \text{vec} \left[ \mathbf{S} \frac{d\mathbf{S}}{dj} + \frac{d\mathbf{S}}{dj} \mathbf{S} \right] + \frac{2\phi - \sin(2\phi)}{r^3} \text{vec} \left[ \frac{d\mathbf{S}}{dj} \right] + \frac{2k(1 - \cos(2\phi) - \phi \sin(2\phi))}{r^3} \text{vec}[\mathbf{S}] + \frac{3k \sin(2\phi) - 2k\phi(2 + \cos(2\phi))}{r^4} \text{vec}[\mathbf{S}^2] \quad (19)$$

where three such equations are required for  $j \in \{x, y, z\}$  and the derivatives of  $\mathbf{S}$  are derived algebraically from Eq. (16).

Since the directional derivatives of Eq. (17) and Eq. (18), together with time-propagators of Eq. (7), do not involve any matrix operations, other than a few trivial multiplications, ESCALADE offers substantial computational gains relative to the AUXMAT method in Eq. (14).

## III. ACCELERATED NEWTON-RAPHSON OPTIMAL CONTROL

Moving away from a chosen calculation method of directional propagator derivatives, the remaining bottleneck of the

Newton-Raphson methods presented above is the off-diagonal Hessian elements; the mixed derivatives of Eq. (13).

As a starting point, ESCALADE includes an additional efficiency, which also applies to the AUXMAT method, where the central effective propagator in Eq. (13) can be split to  $\mathbf{U}_{m+1}^{n-1} = \mathbf{U}_{m+1}^{n-1} \mathbf{U}_1^m \mathbf{U}_m^1 = \mathbf{U}_1^{n-1} \mathbf{U}_m^1$ , Eq. (13) becomes

$$\nabla^2 \mathcal{F}(c_{k,n}, c_{j,m}) = \text{Re} \langle \hat{\chi}_{n+1} D_{k,n} | \mathbf{U}_1^{n-1} \mathbf{U}_m^1 | D_{j,m} \hat{\rho}_{m-1} \rangle \quad (20)$$

An interpretation of these two central effective propagators is: the right hand side,  $\langle \hat{\chi}_{n+1} D_{k,n} |$ , is multiplied by the effective propagator  $\mathbf{U}_1^{n-1}$ , presenting the directional derivative of  $t_n$  to be evaluated at  $t_0$ ; the left hand side,  $| D_{j,m} \hat{\rho}_{m-1} \rangle$ , is multiplied by the time-reversed effective propagator  $\mathbf{U}_m^1$ , presenting the directional derivative of  $t_m$  to also be evaluated at  $t_0$ .

To outline how this can be overcome, a representation of a *trajectory* is introduced:

$$[\boldsymbol{\rho}]_m^n \triangleq [|\hat{\rho}_n\rangle \quad |\hat{\rho}_{n-1}\rangle \quad \cdots \quad |\hat{\rho}_{m+1}\rangle \quad |\hat{\rho}_m\rangle] \quad (21)$$

which is an array of column vectors and the whole trajectory from the dynamics in Eq. (3) is contained in  $[\boldsymbol{\rho}]_0^N$ . Trajectory analysis is useful for visualising pulse dynamics [51]. Taking the concept of a single matrix containing all trajectory information, a *directional derivative trajectory*, evaluated at  $t_0$  as with the right side of Eq. (20), can be defined as

$$[\partial_j^{[0]} \boldsymbol{\rho}]_0^n \triangleq [|\mathbf{U}_n^1 D_{j,n} \hat{\rho}_{n-1}\rangle \quad \cdots \quad |\mathbf{U}_2^1 D_{j,2} \hat{\rho}_1\rangle \quad |\mathbf{U}_1^1 D_{j,1} \hat{\rho}_0\rangle] \quad (22)$$

where the superscript  $^{[0]}$  is used to indicate evaluation at  $t_0$ .

With the realisation that a *directional derivative trajectory* in Eq. (22) is a matrix in itself,  $n$  Hessian elements can be calculated with one matrix-vector product with

$$\begin{bmatrix} \nabla^2 \mathcal{F}(c_{k,n}, c_{j,n}) \\ \vdots \\ \nabla^2 \mathcal{F}(c_{k,n}, c_{j,2}) \\ \nabla^2 \mathcal{F}(c_{k,n}, c_{j,1}) \end{bmatrix}^T = \text{Re} \langle \hat{\chi}_{n+1} D_{k,n} \mathbf{U}_1^{n-1} | \overbrace{[\partial_j^{[0]} \boldsymbol{\rho}]_0^n}^{N \text{ times forward}} \underbrace{|}_{N \text{ times backward}} \rangle \quad (23)$$

Given that the total effective propagator  $\mathbf{U}_1^N$  can be calculated with forward propagation,  $\mathbf{U}_1^{n-1}$  can be updated during subsequent backward propagation with  $\mathbf{U}_1^{n-1} = \hat{P}_{n-1}^\dagger \mathbf{U}_1^n$ . The single vector-matrix product of Eq. (23), per time-slice, is expected to be much more efficient than the  $n - 1$  vector-vector products, per time-slice, in Eq. (13).

#### IV. ACCELERATION OF A BROADBAND MRI EXAMPLE

The authors choose to set the test of the method presented above in the context of MRI because there is a very real need to have computationally fast OC methods to run *on-the-fly* with a need for patient specific solutions. Often, OC-facilitated MRI exploits simultaneous/parallel control systems e.g. eight radiofrequency channels (x- and y-controls) [14, 52] and three magnetic field gradients and/or numerous local shims (z-controls) [40, 52, 53].

The optimisation is set as robust for an ensemble of 101 spin- $\frac{1}{2}$  systems, with offset bandwidth  $\frac{\omega}{2\pi} \in [-\frac{1}{2}, +\frac{1}{2}]$  kHz, simulated using a single block-diagonal Liouvillian with each block operating on a single ensemble member [37, 41].

The time-slice,  $\Delta t$ , is often fixed to the hardware digitalisation dwell-time: typically a few  $\mu\text{s}$ . Modern MRI systems handle  $N > 1000$ , but the pulse duration,  $T = N\Delta t$ , is usually kept around a few ms to avoid degradation of pulse performance due to transverse relaxation. As a set of speed tests, these three variables are incremented and set as a range of OC problems and are shown in Fig. 2. The vertical dashed lines indicate a set of variables physically relevant to MRI.

Figure 2 shows the average speedup of the accelerated auxiliary matrix method (*acc-AUXMAT*) and the accelerated ESCALADE method (*acc-ESCALADE*), both relative to the standard auxiliary matrix method. A separate fidelity, gradient, and Hessian calculation is performed for each method from a random control waveform, with  $c_x$ ,  $c_y$ , and  $c_z$  controls in the order of  $2\pi \times 10^3 \text{ rad s}^{-1}$ . The average is over 84 different random control pulses, run in parallel on 28 CPU cores.

Figure 2A shows that the effect of increasing  $T$  while also increasing  $\Delta t$  is, approximately, a constant speedup of *acc-AUXMAT* and *acc-ESCALADE* Hessian. This can be attributed to the effective propagator splitting of Eq. (20). The small speedup of *acc-AUXMAT* fidelity and gradient calculations is due to an algorithmic efficiency from coding in a way that lends itself to the accelerated Hessian methods.

The main result of this manuscript is the speedup of Hessian calculations of the *acc-AUXMAT* and *acc-ESCALADE* methods, with speedup increasing as  $N$  increases, in Fig. 2B and Fig. 2C, to over  $\times 100$  when a large  $N$  is used. Furthermore, this trend does not appear to dampen, indicating further speedup when  $N \gg 1000$ .

From the evidence in Fig. 2B and Fig. 2C, the accelerated Hessian calculations of Eq. (23) do indeed remove the  $\mathcal{O}(N^2)$  scaling of the original Newton-Raphson method [31], reducing to a linear scaling  $\mathcal{O}(N)$ .

#### V. CONCLUSION

A new mathematical formulation of the Newton-Raphson GRAPE method [31] has been presented in Liouville space and applies to optimal control problems with unitary evolution. The ESCALADE method [44] recast the cumbersome problem of finding derivatives – using trigonometric evaluations of vectorised arrays rather than matrix-matrix products and computationally expensive matrix exponentials – and factorised the central propagator to avoid  $\mathcal{O}(N^2)$  scaling, now reduced to  $\mathcal{O}(N)$ , in the computation of the Hessian. The ESCALADE method is shown in a new light of Liouville space, with the additional derivation of z-controls, which are important to MRI.

The main result is a new formulation of the Newton-Raphson GRAPE method in Liouville space, being an optimisation method with quadratic convergence to an optimal solution, reducing the expensive polynomial scaling of the control problem to a linear scaling when increasing the number of

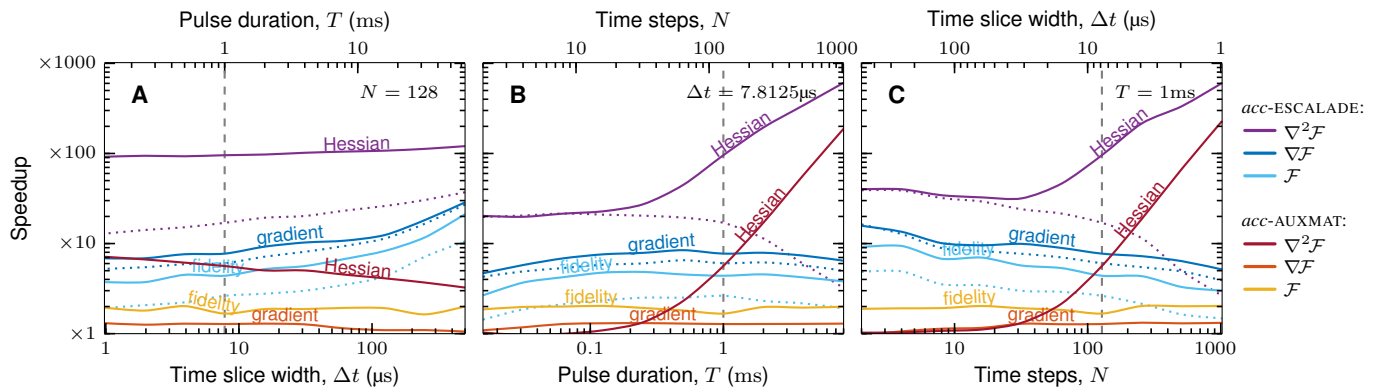


FIG. 2. The average speedup of the accelerated ESCALADE method (*acc*-ESCALADE) and the accelerated auxiliary matrix method (*acc*-AUXMAT), compared to the auxiliary matrix method. The number of time-steps,  $N$ , the time-slice width,  $\Delta t$ , and the pulse duration,  $T$ , are parameters affecting computation time. In each of the three plots one parameter is kept constant: (A)  $N = 128$ , (B)  $\Delta t = 7.8125 \mu\text{s}$ ; and (C)  $T = 1 \text{ ms}$ . The dotted lines in each plot show the speedup of *acc*-ESCALADE relative to *acc*-AUXMAT.

piecewise-constant pulses in optimal solution. Speedup increases as the number of time-slices,  $N$ , increases:  $\times 4$  to  $\times 200$ , for  $N = 100$  and  $N = 1000$  respectively. Furthermore, employing ESCALADE within this new Hessian calculation method shows further speedup of  $\times 70$  to  $\times 600$ , for  $N = 100$  and  $N = 1000$  respectively, when compared to the original Newton-Raphson GRAPE method.

## ACKNOWLEDGMENTS

DLG thanks Pranav Singh and Mohammadali Foroozandeh for useful discussions on the ESCALADE method, Burkhard Luy for his continued support, and Martin Goodwin for proof-reading.

MSV would like to thank Villum Fonden, Eva og Henry Fraenkels Mindefond, Harboefonden, and Kong Christian Den Tiendes Fond.

- 
- [1] S. J. Glaser, U. Boscain, T. Calarco, C. P. Koch, W. Köckenberger, R. Kosloff, I. Kuprov, B. Luy, S. Schirmer, T. Schulte-Herbrüggen, D. Sugny, and F. K. Wilhelm, Training schrödinger's cat: quantum optimal control, *Eur. Phys. J. D* **69**, 279 (2015).
- [2] A. Acín, I. Bloch, H. Buhrman, T. Calarco, C. Eichler, J. Eisert, D. Esteve, N. Gisin, S. J. Glaser, F. Jelezko, S. Kuhr, M. Lewenstein, M. F. Riedel, P. O. Schmidt, R. Thew, A. Wallraff, I. Walmsley, and F. K. Wilhelm, The quantum technologies roadmap: a european community view, *New J. Phys.* **20**, 080201 (2018).
- [3] J. C. Saywell, I. Kuprov, D. Goodwin, M. Carey, and T. Freegarde, Optimal control of mirror pulses for cold-atom interferometry, *Phys. Rev. A* **98**, 023625 (2018).
- [4] J. C. Saywell, *Optimal control of cold atoms for ultra-precise quantum sensors*, Ph.D. thesis, University of Southampton, UK (2020).
- [5] J. Saywell, M. Carey, M. Belal, I. Kuprov, and T. Freegarde, Optimal control of raman pulse sequences for atom interferometry, *J. Phys. B: At. Mol. Opt. Phys.* **53**, 085006 (2020).
- [6] J. Saywell, M. Carey, N. Dedes, I. Kuprov, and T. Freegarde, Can optimised pulses improve the sensitivity of atom interferometers?, in *Quantum Technology: Driving Commercialisation of an Enabling Science II*, Vol. 11881, edited by M. J. Padgett, K. Bongs, A. Fedrizzi, and A. Politi, International Society for Optics and Photonics (SPIE, 2021) pp. 83–92.
- [7] J. Zhang, R. Laflamme, and D. Suter, Experimental implementation of encoded logical qubit operations in a perfect quantum error correcting code, *Phys. Rev. Lett.* **109**, 100503 (2012).
- [8] G. Waldherr, Y. Wang, S. Zaiser, M. Jamali, T. Schulte-Herbrüggen, H. Abe, T. Ohshima, J. Isoya, J. F. Du, P. Neumann, and J. Wrachtrup, Quantum error correction in a solid-state hybrid spin register, *Nature* **506**, 204 (2014).
- [9] F. Dolde, V. Bergholm, Y. Wang, I. Jakobi, B. Naydenov, S. Pezzagna, J. Meijer, F. Jelezko, P. Neumann, T. Schulte-Herbrüggen, J. Biamonte, and J. Wrachtrup, High-fidelity spin entanglement using optimal control, *Nat. Commun.* **5**, 3371 (2014).
- [10] N. Khaneja, R. Brockett, and S. J. Glaser, Time optimal control in spin systems, *Phys. Rev. A* **63**, 032308 (2001).
- [11] T. E. Skinner, T. O. Reiss, B. Luy, N. Khaneja, and S. J. Glaser, Application of optimal control theory to the design of broadband excitation pulses for high-resolution NMR, *J. Magn. Reson.* **163**, 8 (2003).
- [12] N. Khaneja, T. Reiss, C. Kehlet, T. Schulte-Herbrüggen, and S. J. Glaser, Optimal control of coupled spin dynamics: design of NMR pulse sequences by gradient ascent algorithms, *J. Magn. Reson.* **172**, 296 (2005).
- [13] Z. Tošner, S. J. Glaser, N. Khaneja, and N. C. Nielsen, Effective Hamiltonians by optimal control: Solid-state NMR double-quantum planar and isotropic dipolar recoupling, *J. Chem. Phys.* **125**, 184502 (2006).
- [14] M. S. Vinding, D. Brenner, D. H. Y. Tse, S. Vellmer, T. Vosegaard, D. Suter, T. Stöcker, and I. I. Maximov, Applica-

- tion of the limited-memory quasi-Newton algorithm for multi-dimensional, large flip-angle RF pulses at 7T, *Magn. Reson. Mater. Phys.* **30**, 29 (2017).
- [15] E. V. Reeth, H. Ratiney, K. Tse Ve Koon, M. Tesch, D. Grenier, O. Beuf, S. J. Glaser, and D. Sugny, A simplified framework to optimize MRI contrast preparation, *Magn. Reson. Med.* **81**, 424 (2019).
- [16] J. Somló, V. A. Kazakov, and D. J. Tannor, Controlled dissociation of  $I_2$  via optical transitions between the X and B electronic states, *Chem. Phys.* **172**, 85 (1993).
- [17] W. Zhu, J. Botina, and H. Rabitz, Rapidly convergent iteration methods for quantum optimal control of population, *J. Chem. Phys.* **108**, 1953 (1998).
- [18] Y. Maday and G. Turinici, New formulations of monotonically convergent quantum control algorithms, *J. Chem. Phys.* **118**, 8191– (2003).
- [19] R. Eitan, M. Mundt, and D. J. Tannor, Optimal control with accelerated convergence: Combining the Krotov and quasi-Newton methods, *Phys. Rev. A* **83**, 053426 (2011).
- [20] P. Doria, T. Calarco, and S. Montangero, Optimal control technique for many-body quantum dynamics, *Phys. Rev. Lett.* **106**, 190501 (2011).
- [21] N. Rach, M. M. Müller, T. Calarco, and S. Montangero, Dressing the chopped-random-basis optimization: A bandwidth-limited access to the trap-free landscape, *Phys. Rev. A* **92**, 062343 (2015).
- [22] G. Ciaramella, A. Borzi, G. Dirr, and D. Wachsmuth, Newton methods for the optimal control of closed quantum spin systems, *SIAM J. Sci. Comput.* **37**, A319 (2015).
- [23] S. Machnes, E. Assémat, D. Tannor, and F. K. Wilhelm, Tunable, flexible, and efficient optimization of control pulses for practical qubits, *Phys. Rev. Lett.* **120**, 150401 (2018).
- [24] D. Lucarelli, Quantum optimal control via gradient ascent in function space and the time-bandwidth quantum speed limit, *Phys. Rev. A* **97**, 062346 (2018).
- [25] D. Quiñones Valles, S. Dolgov, and D. Savostyanov, Tensor product approach to quantum control, in *Integral Methods in Science and Engineering: Analytic Treatment and Numerical Approximations*, edited by C. Constanda and P. Harris (Springer, 2019) pp. 367–379.
- [26] S. Conolly, D. Nishimura, and M. A., Optimal control solutions to the magnetic resonance selective excitation problem, *IEEE Trans. Med. Imaging* **5**, 106 (1986).
- [27] J. Mao, T. H. Mareci, K. N. Scott, and E. R. Andrew, Selective inversion radiofrequency pulses by optimal control, *J. Magn. Reson.* **70**, 310 (1986).
- [28] L. Viola and S. Lloyd, Dynamical suppression of decoherence in two-state quantum systems, *Phys. Rev. A* **58**, 2733 (1998).
- [29] L. Viola, E. Knill, and S. Lloyd, Dynamical decoupling of open quantum systems, *Phys. Rev. Lett.* **82**, 2417 (1999).
- [30] P. de Fouquieres, S. G. Schirmer, S. J. Glaser, and I. Kuprov, Second order gradient ascent pulse engineering, *J. Magn. Reson.* **212**, 412 (2011).
- [31] D. L. Goodwin and I. Kuprov, Modified Newton-Raphson GRAPE methods for optimal control of spin systems, *J. Chem. Phys.* **144**, 204107 (2016).
- [32] A. N. Pechen and D. J. Tannor, Are there traps in quantum control landscapes?, *Phys. Rev. Lett.* **106**, 120402 (2011).
- [33] K. Kobzar, T. E. Skinner, N. Khaneja, S. J. Glaser, and B. Luy, Exploring the limits of broadband excitation and inversion pulses, *J. Magn. Reson.* **170**, 236 (2004).
- [34] K. Kobzar, T. E. Skinner, N. Khaneja, S. J. Glaser, and B. Luy, Exploring the limits of broadband excitation and inversion: II. RF-power optimized pulses, *J. Magn. Reson.* **194**, 58 (2008).
- [35] D. L. Goodwin, *Advanced optimal control methods for spin systems*, Ph.D. thesis, University of Southampton, UK (2017).
- [36] Z. Tošner, M. J. Brandl, J. Blahut, S. J. Glaser, and B. Reif, Maximizing efficiency of dipolar recoupling in solid-state NMR using optimal control sequences, *Sci. Adv.* **7**, eabj5913 (2021).
- [37] I. Kuprov, Fokker-Planck formalism in magnetic resonance simulations, *J. Magn. Reson.* **270**, 124 (2016).
- [38] M. S. Vinding, B. Skyum, R. Sangill, and T. E. Lund, Ultrafast (milliseconds), multidimensional RF pulse design with deep learning, *Magn. Reson. Med.* **82**, 586 (2019).
- [39] M. S. Vinding, C. S. Aigner, S. Schmitter, and T. E. Lund, DeepControl: 2DRF pulses facilitating inhomogeneity and B0 off-resonance compensation in vivo at 7T, *Magn. Reson. Med.* **85**, 3308 (2021).
- [40] M. S. Vinding, D. L. Goodwin, I. Kuprov, and T. E. Lund, Optimal control gradient precision trade-offs: Application to fast generation of DeepControl libraries for MRI, *J. Magn. Reson.* **333**, 107094 (2021).
- [41] D. L. Goodwin, M. R. M. Koos, and B. Luy, Second order phase dispersion by optimised rotation pulses, *Phys. Rev. Research* **2**, 033157 (2020).
- [42] J. D. Haller, D. L. Goodwin, and B. Luy, SORDOR pulses: expansion of the Böhlen-Bodenhausen scheme for low-power broadband magnetic resonance, *Magn. Reson.* **3**, 53 (2022).
- [43] M. F. Dempsey, B. Condon, and D. M. Hadley, MRI safety review, in *Seminars in Ultrasound, CT and MRI*, Vol. 23 (2002) pp. 392–401.
- [44] M. Foroozandeh and P. Singh, Optimal control of spins by analytical Lie algebraic derivatives, *Automatica* **129**, 109611 (2021).
- [45] W. Kallies, *Concurrent optimization of robust refocused pulse sequences for magnetic resonance spectroscopy*, Ph.D. thesis, Technische Universität München, DE (2018).
- [46] D. L. Goodwin and I. Kuprov, Auxiliary matrix formalism for interaction representation transformations, optimal control, and spin relaxation theories, *J. Chem. Phys.* **143**, 084113 (2015).
- [47] D. J. Siminovitch, Rotations in NMR: Part I. Euler-Rodrigues parameters and quaternions, *Concepts Magn. Reson.* **9**, 149 (1997).
- [48] S. J. Glaser, T. Schulte-Herbrüggen, M. Sieveking, O. Schedletsky, N. C. Nielsen, O. W. Sørensen, and C. Griesinger, Unitary control in quantum ensembles: Maximizing signal intensity in coherent spectroscopy, *Science* **280**, 421 (1998).
- [49] C. F. Van Loan, Computing integrals involving the matrix exponential, *IEEE Trans. Automat. Contr.* **23**, 395 (1978).
- [50] D. L. Goodwin, P. Singh, and M. Foroozandeh, Adaptive optimal control of entangled qubits (2022), accepted for publication in *Sci. Adv.*
- [51] I. Kuprov, Spin system trajectory analysis under optimal control pulses, *J. Mag. Reson.* **233**, 107 (2013).
- [52] M. Vinding, B. Guérin, T. Vosegaard, and N. Nielsen, Local SAR, global SAR, and power-constrained large-flip-angle pulses with optimal control and virtual observation points, *Magnetic Resonance in Medicine* **77**, 374 (2017).
- [53] J. P. Stockmann and L. L. Wald, In vivo  $B_0$  field shimming methods for MRI at 7 T, *NeuroImage* **168**, 71 (2018).